Bone remodelling model including overload simulation

Bernardo Afonso Rodrigues
bernardo.f.rodrigues@tecnico.ulisboa.pt

Instituto Superior Técnico, Lisboa, Portugal

March 2017

Abstract

Bone is a dynamic tissue that adapts its form, size and structure to the mechanical environment. According to Julius Wolff, bone density increases if the mechanical stimulus is high and it decreases if it is low. This behavior has been modelled computationally, using mathematical models, called bone remodelling models. However, under extreme mechanical conditions, bone density may decrease due to excessive stimulus, which is not present in the majority of the mathematical models developed. This phenomenon is called overload resorption.

In this work, a novel mathematical model is proposed for bone remodelling, using strain as mechanical stimulus, which takes in consideration bone resorption due to overload. The performance of this model is evaluated and compared to existing models in the literature. For this, finite element models of a femur (two and three-dimensional) are used, with and without prostheses implanted. The mathematical models are tested with and without overload incorporated and the differences obtained are analyzed.

The results obtained using both mathematical models are qualitatively similar and it is possible to observe bone resorption due to overload, mainly in bone regions contacting with the prosthesis. It is also possible to conclude that the overload phenomenon is more prominent when the prosthesis is implanted in low density bone.

The work developed allowed to simulate bone resorption due to overload. However, the mathematical model should be further tested, using more complex finite element models to assure its good performance in real case studies.

Keywords: Bone remodelling model, Bone overload, Finite element method, Computational Mechanics.

1. Introduction

In 1982, Julius Wolff theorized that bone can either be formed or absorbed in different regions, depending on the load applied [1]. These changes contribute to bone homeostasis. In a healthy condition, there is an equilibrium between bone absorption and bone formation. However, if the mechanical environment is disturbed, bone integrity may be compromised. For example, bone density decreases due to prolonged periods of inactivity, which makes the bone weaker and more prone to injuries and fractures. On the other hand, when submitted to high loads (within a certain range), the bone becomes denser [2].

Over the last decades, several mathematical models have been developed to simulate bone adaptation to the mechanical environment [3, 4, 5]. These models are, in most cases, locally regulated by a mechanical stimulus (that vary between models) [6] and are composed of three regions: a stationary region or dead zone, in which no bone absorption or formation occurs, a bone resorption region and bone formation region. In most models, the bone formation region is not limited, i.e., the higher the stimulus, the higher the bone formation rate [7], which is not physiological because under excessive loads, damage may accumulate faster than the bone is able to recover, leading to bone absorption instead of bone formation [8]. Models that can simulate bone resorption due to overloading are needed to be able to predict the bone adaptation process under more critical conditions, such as in the presence of implants. Some work has been done in this area, such as the models developed by Crupi et al. [9] and Li et al. [10]. However, bone overloading phenomenon is no yet well comprehended and further studies need to be done in this subject.

In this work, a novel mathematical model for bone remodeling that takes in consideration bone resorption due to overload, based on the theory developed by Frost [11], is proposed. The performance of this model is tested under normal conditions (without overload) and under overload conditions and compared with the model developed by Li et al. [10].

2. Background

2.1. Bone anatomy

Along with cartilage, tendons and ligaments, bones are part of the skeletal system, which has a variety of functions in the human body. It serves as a framework where muscles and other tissues are attached, providing support and maintaining the shape of the body, protects vital organs from injury, such as the brain and heart, allows movement of the body by acting as levers between muscles and favoring the use of forces generated by them, serves as a reservoir of minerals, such as calcium and phosphorus, releases them when needed and enables haematopoiesis, which is the production of red blood cells, in the bone marrow [12].

At the macroscopic structure, there are two types of bone: high density bone, called cortical or compact bone and low density bone called trabecular, spongy or cancellous bone.

Concerning the histology of the bone, there are three types of cells: osteoblasts, osteoclasts and osteocytes. Osteoblasts come from osteoprogenitor cells and are bone forming cells (they are responsible for synthesizing the organic components of the bone matrix, such as collagen type I and proteoglycans) and are found in bone growing regions. When osteoblasts are surrounded by the osteoid matrix produced by themselves, they become osteocytes. Osteocytes are the most abundant bone cells and are involved in the maintenance of bone matrix, by controlling the activity of osteoblasts and osteoclasts within a basic multicellular unit (BMU). Each cell is in a lacuna that contact with adjacent cells via gap junctions. Lastly, osteoclasts are multinucleated cells responsible for bone resorption and derive from monocytes and macrophages. They have a much shorter life than osteoblasts, but their effect dominates over that of osteoblasts because they absorb bone faster than osteoblasts synthesize it. The balance between the activity of these two cells is responsible for the ongoing modelling and remodelling processes of the bone. [13, 12]

2.2. Bone remodelling

Bone modelling is the alteration of bone size and shape. It consists of either bone formation (osteoblast activity) or bone resorption (osteoclast activity), occurring independently at different sites. On the other hand, bone remodelling is the result of sequential actions at the same site of both bone-degrading osteoclasts and bone-forming osteoblasts, called the bone remodelling units. It is crucial to maintain the integrity of the skeleton because it repairs the micro-damage caused by the stress that bone is subjected in everyday activities and to regulate mineral homeostasis [14].

According to Wolffs Law [1], bone will change in response to the loads that it is subjected. This implies that if load increases in a particular region, the bone will remodel to become stronger and support that load. The opposite also occurs: if the load decreases, the bone will remodel itself to become less dense, given the lack of stimulus [15]. This last phenomenon may result in osteopenia, a frequent problem when a prosthesis is implanted [16].

Chemical stimulus can also trigger bone remodelling by means of hormones and growth factors that either activate or supress the bone remodelling units (e.g. fibroblast growth factor activates osteoclasts and osteoblasts and insulin-like growth factors activate osteocytes) [17].

While the bone remodelling process is taking place, osteoblasts and osteoclasts are arranged within anatomical structures, the basic multicellular units, delimited by cells. A BMU consists of osteoclasts in front, followed by osteoblasts in the tail. Bone remodelling takes essentially five steps [17]:

- Activation Phase - consists on the detection of the signal (mechanical or chemical);
- Resorption Phase - osteoclast precursors differentiate and osteoclasts resorb the bone, with the creation of a sealed zone;
- Reversal Phase - preparation of the zone to osteoblast activity, by removal of the collagen matrix covering the sealed zone;
- Formation Phase bone formation by secretion of molecules that will form the bone (e.g. collagen type I, proteoglycans and glycosylated proteins);
- Termination Phase The conclusion of the remodelling cycle. Mature osteoblasts undergo apoptosis or differentiate into osteocytes.

A schematic representation of this process can be observed in Figure 1.

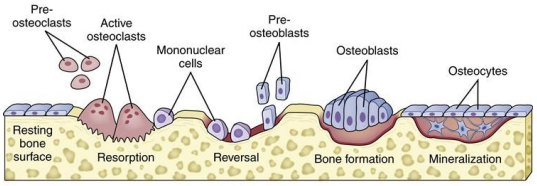

Figure 1: Schematic representation of the bone remodelling process. Adapted from [18].

The remodelling process is very complex and rely on the sequential and cooperative activity of osteoblasts and osteoclasts. Deregulation of this process may be connected to some diseases such as osteoporosis and can bring serious problems [19].

2.3. Bone overloading

According to Julius Wolff, high mechanical loads tend to promote bone formation and increase bone density. However, it has been proved that, above a certain load, the damage accumulated in the bone is higher than the recovery which will result in bone loss [20]. This way, in excessive load regions bone degradation occurs, leading to bone density decrease, which is called bone overloading [10]. This phenomenon can also alter the density distributions of the surrounding bone tissue which will impact the whole bone. Moreover, excessive loads in an implanted bone may lead to large motions between prosthesis and bone, resulting in loosening of the implant [21].

The overload phenomenon is not yet well comprehended and is of crucial importance when analyzing extraordinary load cases such as prostheses implants.

3. Implementation

In this work, two mathematical models are applied to replicate the bone remodelling process, including bone resorption due to overload. The main difference between the models is the mechanical stimulus considered. In parallel to the mathematical model, finite element analyses are performed, in the software *ABAQUS*, to assess the mechanical environment of bone. Iterative procedures, based on Euler and Runge-Kutta methods, are adopted to solve the differential equations of the bone remodelling models. In each iteration, the mechanical stimulus obtained in the finite element analysis is used in the mathematical model. Then, the density distribution obtained in the mathematical model is used in ABAQUS for the finite elements analysis. The iterations are repeated until the average density variation is under 0.001 $g \cdot cm^{-3}$. This chapter presents the computational framework for the simulation of the bone remodelling process including overload.

3.1. Mathematical Models for bone remodelling

Strain energy density model

This model was developed by Li et al. [10] and uses strain energy density as the mechanical stimulus. The differential equation that rules the model is expressed by:

$$\frac{d\rho}{dt} = B(\frac{U}{\rho} - k) - D(\frac{U}{\rho} - k)^2 \qquad (1)$$

where B, D and k are constants, with the following units: $[k] = J \cdot g^{-1}$, $[B] = (g \cdot cm^{-3})^2(MPa \cdot timeunit)^{-1}$ and $[D] = (g \cdot cm^{-3})^3 MPa^{-2}(timeunit)^{-1}$. U is the strain energy density and ρ is the bone density which is limited between 0.01 $g \cdot cm^{-3}$ and 1.74 $g \cdot cm^{-3}$. The second order term, in Equation 1 adds the overload phenomenon to the model, in high load regions. The constant k is the threshold value for the stimulus, i.e., the strain energy density above which the density increases and below which it decreases (without taking in consideration the overload region), whereas $\frac{B}{D} + k$ is the threshold for the overload region, i.e., above this threshold overload resorption occurs and bone density decreases. It is easy to conclude that for higher values of D, overload will occur for lower values of strain energy density.

Figure 2 illustrates the change in bone density rate expressed in Equation 1.

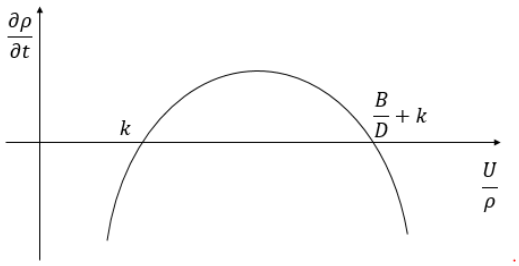

Figure 2: Bone density rate as a function of the mechanical stimulus $\frac{U}{\rho}$ according to the bone remodelling model developed by Li et al. [10].

The Euler method formulation of this model is:

$$\rho_{t+\Delta t} = \rho_t + \Delta t(B(\frac{U}{\rho_t} - k) - D(\frac{U}{\rho_t} - k)^2) \qquad (2)$$

On the other hand, the implementation of the second order Runge-Kutta method is more complex. An intermediate step needs to be performed to compute a new density, ρ_m, given by:

$$\rho_m = \rho_t + \frac{\Delta t}{2}(B(\frac{U_t}{\rho_t} - k) - D(\frac{U_t}{\rho_t} - k)^2) \qquad (3)$$

Because of this, the Second Order Runge-Kutta method is more time consuming than the Euler Method - for each iteration, two finite elements analyses need to be performed. Then, ρ_m is used to calculate $\rho_{t+\Delta t}$ as follows:

$$\rho_{t+\Delta t} = \rho_t + \Delta t(B(\frac{U_m}{\rho_m} - k) - D(\frac{U_m}{\rho_m} - k)^2) \qquad (4)$$

Strain-based model

Based on the work developed by Wiskott et al. [22], a novel model was developed using strain as the mechanical stimulus. According to the authors, five strain regions cause different bone density changes:

- strain $< 100\mu\varepsilon$ - Strains in this range cause bone resorption due to disuse;

- $100\mu\varepsilon <$ strain $< 2000\mu\varepsilon$ - Strains in this range do not change bone density;
- $2000\mu\varepsilon <$ strain $< 4000\mu\varepsilon$ - Strains in this range cause bone formation due to stimulation;
- $4000\mu\varepsilon <$ strain $< 20000\mu\varepsilon$ - Strains in this range cause pathological overload due to excessive load i.e., bone density decreases;
- strain $> 20000\mu\varepsilon$ - Strains in this range cause bone fracture.

Considering all these regions, the following bone remodelling law was defined:

$$\frac{d\rho}{dt} = \begin{cases} B(\psi - \varepsilon_1), & \text{if } \varepsilon < \varepsilon_1 \\ 0, & \text{if } \varepsilon_1 < \varepsilon < \varepsilon_2 \\ B(\psi - \varepsilon_2), & \text{if } \varepsilon_2 < \varepsilon < \varepsilon_3 \\ B(\varepsilon_4 - \psi), & \text{if } \varepsilon_3 < \varepsilon < \varepsilon_5 \\ \text{Fracture}, & \text{if } \varepsilon > \varepsilon_5 \end{cases} \quad (5)$$

where ψ is the stimulus considered and ε_i, with $0 < i < 6$, are the strains that delimit the different steps of the model. $\varepsilon_1 = 4{\cdot}10^{-4}$, $\varepsilon_2 = 2{\cdot}10^{-3}$, $\varepsilon_3 = 3{\cdot}10^{-3}$, $\varepsilon_4 = 4{\cdot}10^{-3}$, $\varepsilon_5 = 2{\cdot}10^{-2}$. The bone density change rate as a function of strain (representation of the model) is presented in figure 3.

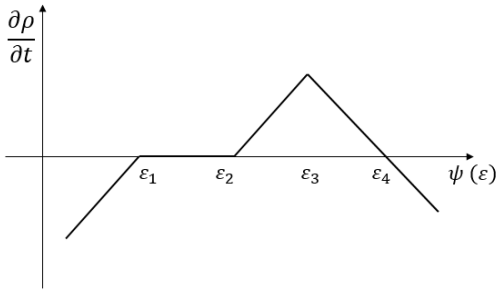

Figure 3: Bone density rate as a function of the mechanical stimulus $\psi(\varepsilon)$ according to the bone remodelling model developed in this work.

Considering strain as the driving force, two different stimuli are considered:

$$\psi_1 = max(|\varepsilon_{max}|, |\varepsilon_{med}|, |\varepsilon_{min}|) \quad (4.4.a)$$

$$\psi_2 = |\varepsilon_{max}| + |\varepsilon_{med}| + |\varepsilon_{min}| \quad (4.4.b)$$

where ε_{max} is the maximal principal strain, ε_{med} is the medium principal strain and ε_{min} is the minimal principal strain. In the two-dimensional case ε_{med} is zero. These two stimuli are chosen based on the work developed by Ruimerman [23].

The Euler method formulation for this model is expressed as:

$$\rho_{t+\Delta t} = \begin{cases} \rho_t + \Delta t \cdot B(\psi_t - \varepsilon_1), & \text{if } \varepsilon < \varepsilon_1 \\ 0, & \text{if } \varepsilon_1 < \varepsilon < \varepsilon_2 \\ \rho_t + \Delta t \cdot B(\psi_t - \varepsilon_2), & \text{if } \varepsilon_2 < \varepsilon < \varepsilon_3 \\ \rho_t + \Delta t \cdot B(\varepsilon_4 - \psi_t), & \text{if } \varepsilon_3 < \varepsilon < \varepsilon_5 \\ \text{Fracture}, & \text{if } \varepsilon > \varepsilon_5 \end{cases} \quad (6)$$

The second-order Runge-Kutta formulation is given by

$$\rho_{t+\Delta t} = \begin{cases} \rho_t + \Delta t \cdot B(\psi_m - \varepsilon_1), & \text{if } \varepsilon < \varepsilon_1 \\ 0, & \text{if } \varepsilon_1 < \varepsilon < \epsilon_2 \\ \rho_t + \Delta t \cdot B(\psi_m - \varepsilon_2), & \text{if } \varepsilon_2 < \varepsilon < \varepsilon_3 \\ \rho_t + \Delta t \cdot B(\varepsilon_4 - \psi_m), & \text{if } \epsilon_3 < \varepsilon < \epsilon_5 \\ \text{Fracture}, & \text{if } \varepsilon > \varepsilon_5 \end{cases} \quad (7)$$

with ψ_m calculated using half of the time step considered i.e., $\frac{\Delta t}{2}$.

3.2. Application cases

To obtain the mechanical stimulus used in the mathematical models and study the changes in bone, finite element analyses are done, both in 2D and 3D. Using the software ABAQUS, different finite element models are developed considering a two-dimensional and a three-dimensional model.

For each model, healthy and prosthetic conditions are modelled, in which bone is intact or is implanted, respectively. The intact bone models are applied to tune the bone remodelling parameters and obtain the bone density distribution close to the biological distribution. The models with prostheses are analyzed using the tuned parameters and the density distribution obtained for the intact bone as initial condition.

In all simulations performed, bone is considered isotropic. Poisson's ratio, ν, is defined as 0.3 and the Young's modulus, E, is given by the following relationship between E and the bone density ρ, according to Carter et al. [24]:

$$E = 3790 \times \rho^3 \quad (8)$$

where ρ, in $g \cdot cm^{-3}$, varies between 0.01 and 1.74 and E is given in MPa.

The interactions between bone and prostheses and bone and side plate were modeled as bonded (Tie, in ABAQUS).

Two-dimensional model

The model of the intact femur, presented in Figure 4.a, is composed of two parts: the femur and a side plate. The side plate, shown in Figure 4.c has three sections of thickness 1 mm, 3 mm and 5 mm (from top to bottom) and it is considered to be made of cortical bone, with Young's Modulus of

17 GPa and Poisson's ratio of 0.3 [27]. It is connected to the bone through a "Tie" constraint to simulate the three-dimensional connectivity of the cortex [28]. The femur has thickness of 40 mm and 3075 quad elements.

The model of the implanted bone, shown in Figure 4.b, has three parts: the femur, the side plate and the prosthesis. The prosthesis is bonded to the femur by a "Tie" constraint and it is made of cobalt-chrome, CoCr, with Poisson's ratio equal to 0.3 and Young's Modulus equal to 230 GPa [29]. The cut femur has 18525 linear quad elements, to be able to capture the rapid changes in the solution.

In both models the bottom nodes are fixed in all directions. Two forces are applied (F_a and F_h) in two reference points, RP-1 (F_a) and RP-2 (F_h), common to both models, to simulate the muscular action and the forces in the articulation. In the intact model, the points RP-1 and RP-2 are connected to the femur and in the implanted femur are connected to the upper left region of the femur and to the head of the implant, respectively. The forces used, presented in Table 1, simulate the forces during the gait cycle [30].

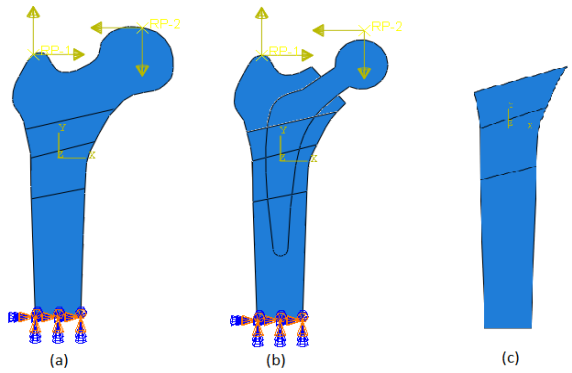

Figure 4: 2D model of the femur: (a) intact bone, (b) implanted bone and (c) side plate.

Table 1: Forces used in the 2D femur model.

Force	F_x	F_y
F_a	768	1210
F_h	-224	-2246

Three-dimensional model

To complement the two-dimensional finite element analyses, three-dimensional finite element models are developed.

A 3D model of a left femur with a resurfacing prosthesis is analyzed. This type of prosthesis is used in patients with hip pathology, leading to osteoarthritis. The pathological bone in the head of the femur is removed and it is shaped to receive the prosthesis, which is fixed to the bone [31]. The CAD model of the intact femur was downloaded from GrabCad [32] and the prosthesis was designed in SolidWorks. Then, both models were imported to the software ABAQUS and the prosthesis was implanted in the femur model. The model of the intact femur, shown in Figure 5.a, is made of one part and it has 28759 tetrahedral elements. The model of the femur with the prosthesis, shown in Figure 5.b is composed of two parts: the femur and the prosthesis. The prosthesis, shown in Figure 5.c, is made of CoCr with Poisson's ratio of 0.3 and Young's modulus of 230 GPa [29] and is bonded to the bone with a "Tie" constraint. The cut femur has 30879 tetrahedral elements.

Similarly to the two-dimensional model, two forces, (F_a and F_h), are applied in two reference points, RP-1 (F_a) and RP-2 (F_h). In the intact model, the points RP-1 and RP-2 are connected to the femur and in the implanted femur are connected to the upper left region of the femur and to the prosthesis, respectively. The forces have the same magnitude and are applied in the same position as in the two-dimensional model. However, in 3D the z component of forces is no longer neglected. Moreover, because in this case a left femur is modelled and in the 2D model a right one is studied, a 180 rotation (along the traditional yy axis) is applied to the forces, which are represented in Table 2. In both models, the nodes at the bottom surface are constrained in all directions.

Table 2: Forces used in the 3D femur model.

Force	F_x	F_y	F_z
F_a	-768	1210	-726
F_h	224	-2246	972

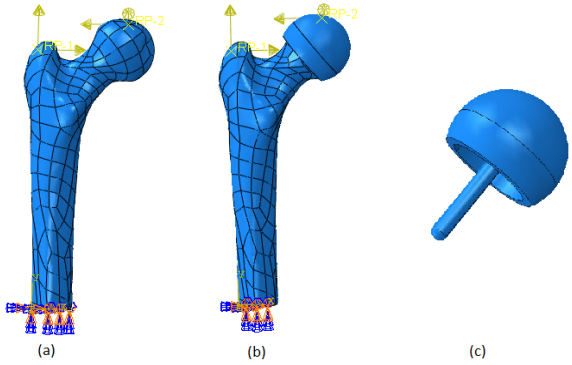

Figure 5: 3D model of the femur: (a) intact bone, (b) implanted bone and (c) prosthesis.

4. Results

The results of the finite element analyses performed using the mathematical remodelling models and finite element models described are now presented.

4.1. Two-dimensional femur model

To analyze the model of the two-dimensional femur two different prostheses are used. Apart from the prosthesis presented in Figure 4, denominated as standard prosthesis, another prosthesis, with larger stem, called large prosthesis, will be tested. The initial density used is presented in Figure 6 and was obtained using both mathematical models without considering overload and the intact two-dimensional femur. Both models based on strain have similar results, so, throughout this work, only the results obtained using $\psi_2 = |\epsilon_{max}| + |\epsilon_{med}| + |\epsilon_{min}|$ are presented and analyzed, considering that the results using ψ_1 are similar.

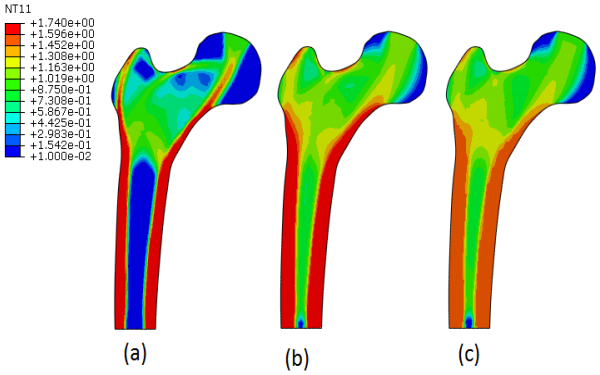

Figure 6: Density distribution obtained in the 2D model of the intact femur: (a) strain energy density model, (b) Strain-based model with ψ_1, (c) Strain-based model with ψ_2 .

Considering the initial density used, presented in Figure 6.a, the large prosthesis is inserted in high density bone (of approximately 1.74 $g \cdot cm^{-3}$), whereas the standard prosthesis is inserted in lower density bone (of approximately 1 $g \cdot cm^{-3}$). This way, the overloading process can also be studied considering the density of the surrounding bone.

For both prostheses, the two mathematical models are tested with and without overload.

The density distributions obtained using the normal prosthesis can be seen in Figure 7.

The results obtained are similar for both mathematical models. The outer region of the diaphysis is composed by high density bone, while the inner region, that is in contact with the prosthesis, is made of medium and low density bone. In the region of transition between methaphysis and diaphysis (metadiaphysis) there are regions of low density bone surrounding the prosthesis. The epiphysis is made of medium density bone with a region of low density. The major differences between incorporating overload or not in the models are located in the region of the diaphysis in contact with the prosthesis: in the model with overload, there is a thin layer

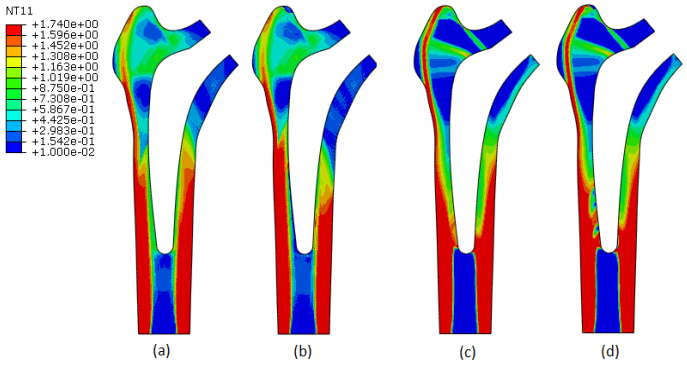

Figure 7: Bone density distribution in the femur with the standard prosthesis obtained using the strain-based model: (a) without overload, (b) with overload and the strain energy density model: (c) without overload, (d) with overload.

of low density bone in this region whereas, in the model without overload, there is medium density bone. The difference of bone density in this region alters the regions surrounding.

The density distributions obtained using the large prosthesis are presented in Figure 8.

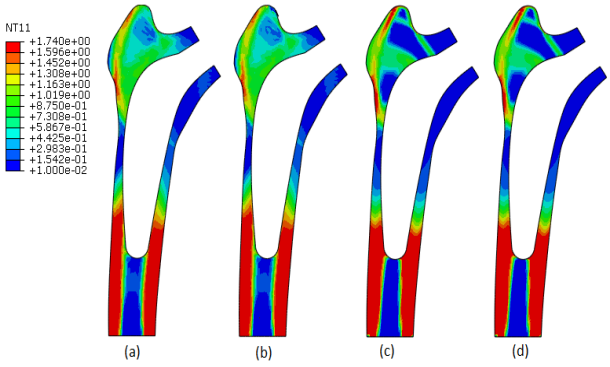

Figure 8: Bone density distribution in the femur with the large prosthesis obtained using the strain-based model: (a) without overload, (b) with overload and the strain energy density model: (c) without overload, (d) with overload.

The results obtained for both models are very similar. There is high density bone in the outer region of the lower part of the diaphysis of the femur, while in the middle and upper part of the diaphysis, there is low density bone. The metaphysis and epiphysis are made of medium density bone with a region of low density. Also, incorporating overload in the mathematical models or not does not change the results considerably, suggesting that overload is not prominent in this situation.

4.2. Three-dimensional femur model

In the following subsection the three-dimensional model of a femur with a resurfacing prosthesis is studied, to complement the results already presented. The intact femur is first analyzed using both mathematical models without overload, so that a proper density distribution can be obtained. The results using the strain based model are presented in Figure 9.

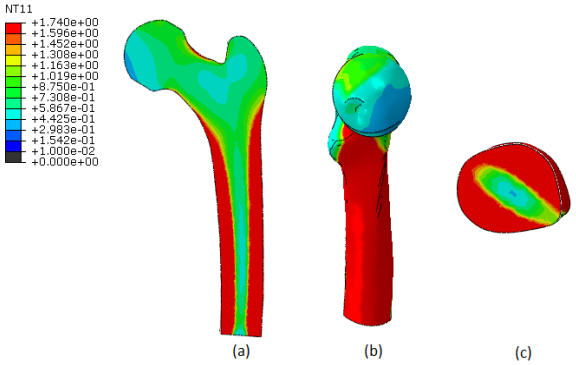

Figure 9: Bone density distribution in the 3D femur obtained using the strain based model: (a) view of a coronal cut, (b) medial view, (c) view of a transversal cut.

The diaphysis of the femur is composed of medium density bone in the inner region, with the center made of low density bone - the medullary canal. The outer region of the diaphysis has high density bone. There is a low density region in the neck of the femur - the Ward's Triangle - and in the lower region of the articular surface. The rest of the femur is composed of medium density bone.

The results obtained using the strain energy density model are presented in Figure 10 . The bone density distribution obtained is similar to that of the strain based model, but the medullary canal is more prominent, presenting a lower density. Also, the femur's head has a higher density bone.

Using the density distributions presented in Figure 9 and Figure 10 as initial conditions, the mathematical models are tested with and without overload, using the finite element model of a femur with a resurfacing prosthesis. The results obtained using the strain based model and the strain energy density models without and with overload are shown in Figure 11 and Figure 12, respectively. The differences worth noting between these results and the ones obtained using the intact femur model are located in the head of the femur, where the prosthesis is implanted. With the bone remodelling model without overload resorption, the density distribution is close to the one obtained in the intact femur, whereas with the model considering overload resorption the density in the head of the femur is decreased, showing bone resorption in these sites.

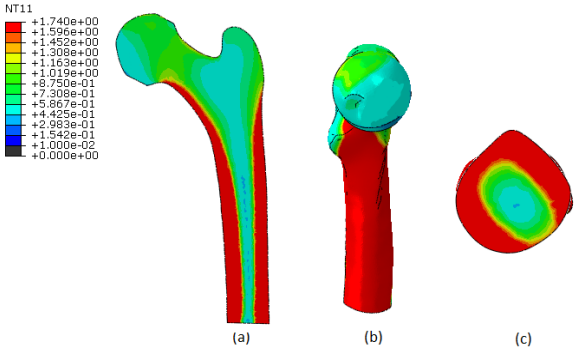

Figure 10: Bone density distribution in the 3D femur obtained using the strain energy density model: (a) view of a coronal cut, (b) medial view, (c) view of a transversal cut.

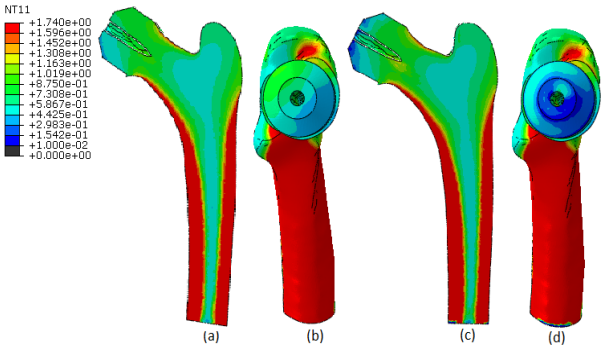

Figure 11: Bone density distribution in the 3D femur with a resurfacing prosthesis obtained using the strain based model without overload (a) view of a coronal cut, (b) medial view and with overload (c) view of a coronal cut, (d) medial view.

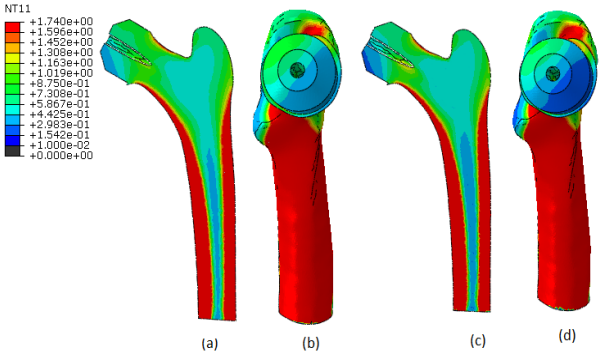

Figure 12: Bone density distribution in the 3D femur with a resurfacing prosthesis obtained using the strain energy density model without overload (a) view of a coronal cut, (b) medial view and with overload (c) view of a coronal cut, (d) medial view.

5. Discussion

Bone remodeling models are very important to study bone adaptation under different mechanical environments. In more critical conditions, bone overloading may occur and influence the bone remodeling process. Some effort has been made in the past few years to incorporate this phenomenon in mathematical models that can simulate bone remodeling [9, 10], which are needed to study bone adaptation under more critical conditions, such as in the presence of implants.

This work focused on developing an alternative bone remodeling model, including overload resorption, using strains as the mechanical stimulus. The performance of this model, described throughout this work as strain-based model, was evaluated under different conditions and it was compared with the model developed by Li et al [10], referred as strain energy density model.

The results obtained confirmed the occurrence of bone overloading in critical conditions (when the prosthesis is implanted in the bone), using both the strain-based model and the strain energy density model. The results obtained applying the two bone remodelling models are similar in most cases.

The strain energy density model was more effective in reproducing the bone density distribution of an intact femur. In fact, the result obtained with the strain energy density model (Figure 6) presents the low density areas in the femur (Ward's triangle and medullary canal), whilst with the strain-based model these areas have a medium density.

Using the two-dimensional femur model with different prostheses implanted, the influence of bone density in the overloading phenomenon could be studied. Implanting the prosthesis in trabecular bone (Figure 7) resulted in a decrease in bone density in the regions adjacent to the prosthesis, when overload was included in the mathematical models. This shows that overload resorption occurred in these regions due to the concentration of high strain and energy. On the other hand, the results obtained when the prosthesis was implanted in high density cortical bone (Figure 8) did not present any differences between the models without and with overload simulation. This suggests that the overload phenomenon may be more prominent in low density bone, which has also been addressed by Crupi et al. [9]. Taking this in consideration, the prosthesis design could be of extreme importance to reduce overload resorption in some cases, that may lead to the prosthesis failure.

The results obtained in the three-dimensional femur model, without the prosthesis, using both mathematical models, are very similar and consistent with the density distribution of a real femur. The improvement of the results compared to the two dimensional model, using the the strain-based model may come from the fact that in three dimensions three strain components are used, instead of only two. In the model with the resurfacing prosthesis, without overload, bone resorption is observed in the femoral head, which is in contact with the prosthesis. According to Ong et al. [33], this result is due to superolateral stress shielding, mostly due to the stress and strain transfered through the stem of the prosthesis. This phenomenon is more prominent in fully bonded prosthesis. So, to reduce bone resorption, the stem may not be fully bonded to the bone. Adding overload to the remodelling model results in a decrease in bone density in the region of the femoral head in contact with the prosthesis, which may result in aseptic loosening, according to Perez et al. [34]. This decrease suggests the existence of overload in this region, which is consistent with the results obtained by Rothstock et al. [35]. In their study, concentrations of strains were found in this particular region, which may cause overload.

In this work a novel bone remodelling model including overload resorption was developed and tested. Some limitations were faced during this process, mostly concerning the lack of information about the overload process which made the validation process difficult. However, bone resorption due to overload was seen and the results were consistent with previous studies.

6. Conclusions

The current work proposed a mathematical model for bone remodelling that takes overload resorption in consideration, using strains as mechanical stimulus. This model was studied using two and three-dimensional finite element models of a femur. Comparisons with the bone remodelling model developed by Li et al [10] were made. The influence of bone density surrounding the prostheses was also studied and some parameters that may influence the models performance were tested.

The density distributions obtained in the intact bones are close to the real ones. Under critical conditions (prosthesis implanted) both mathematical models revealed bone overload resorption near the prostheses due to concentrations of high strains or energies which is in agreement with the literature. Differences between implanting the prosthesis in cortical or trabecular bone were seen: in trabecular bone, overload resorption is more prominent than in cortical bone.

Although the bone remodeling model developed was able to simulate bone overloading, further tests should be done. Because of the fact that the finite element models used in the present work are not very complex, due to several reasons, such as the limited number of load cases considered, future tests

should focus on using more complex finite element models and study the performance of the mathematical model in these cases. Also, cases of bone overloading should be studied in patients and compared to the ones obtained computationally with these models. The fact that the bone overloading phenomenon is not yet well studied which results in lack of information, made the validation of the model hard. With advances in this area, the model should be updated and further validated to follow the novel conclusions.

References

[1] J. Wolff. Das Gesetz der Transformation der Knochen. *Deutsche Medicinische Wochenschrift*, (47):1222–1224, 1892.

[2] Harold M Frost. A 2003 Update of Bone Physiology and Wolff ' s Law for Clinicians. *Angle Orthodontist*, 74(1):3–15, 2004.

[3] S. C. Cowin and D. H. Hegedus. Bone remodeling I: theory of adaptive elasticity. *Journal of Elasticity*, 6(3):313–326, 1976.

[4] G S Beaupré, T E Orr, and D R Carter. An Approach for Time Dependent Bone Modeling and Remodeling- Theoretical Development. *Journal of orthopaedic research*, 8(3):651–661, 1990.

[5] R. Huiskes, H. Weinans, H. J. Grootenboer, M. Dalstra, B. Fudala, and T. J. Slooff. Adaptive bone-remodeling theory applied to prosthetic-design analysis. *Journal of Biomechanics*, 20(11-12):1135–1150, 1987.

[6] H Rodrigues, C Jacobs, J M Guedes, and M P Bendsøe. Global and local material optimization models applied to anisotropic bone adaptation. *IUTAM Symposium on Synthesis in Bio Solid Mechanics*, pages 209–220, 2002.

[7] P. R. Fernandes, J. Folgado, C. Jacobs, and V. Pellegrini. A contact model with ingrowth control for bone remodelling around cementless stems. *Journal of Biomechanics*, 35(2):167–176, 2002.

[8] H M Frost. Bone's mechanostat: A 2003 update. *the Anatomical Record Part a*, 275A(August):1081–1101, 2003.

[9] V Crupi, E Guglielmino, G La Rosa, Jos Vander Sloten, and Hans Van Oosterwyck. Numerical analysis of bone adaptation around an oral implant due to overload stress. *Proceedings of the Institution of Mechanical Engineers, Part H: Journal of Engineering in Medicine*, 218(6):407–415, 2004.

[10] Jianying Li, Haiyan Li, Li Shi, Alex S L Fok, Cemal Ucer, Hugh Devlin, Keith Horner, and Nick Silikas. A mathematical model for simulating the bone remodeling process under mechanical stimulus. *Dental Materials*, 23(9):1073–1078, 2007.

[11] H. M. Frost. Bone Mass and the Mechanostat: A Proposal. *The Anatomical Record*, 219(1):1–9, 1987.

[12] Bart Clarke. Normal bone anatomy and physiology. *Clinical journal of the American Society of Nephrology : CJASN*, 3 Suppl 3:131–139, 2008.

[13] Rinaldo Florencio-silva, Gisela Rodrigues, Estela Sasso-cerri, Manuel Jesus Simões, Paulo Sérgio Cerri, and Bone Cells. Biology of Bone Tissue : Structure , Function , and Factors That Influence Bone Cells. 2015, 2015.

[14] J. C. Crockett, M. J. Rogers, F. P. Coxon, L. J. Hocking, and M. H. Helfrich. Bone remodelling at a glance. *Journal of Cell Science*, 124(7):991–998, 2011.

[15] José Luis Ferretti, Gustavo Roberto Cointry, Ricardo Francisco Capozza, and Harold M. Frost. Bone mass, bone strength, muscle-bone interactions, osteopenias and osteoporoses. *Mechanisms of Ageing and Development*, 124(3):269–279, 2003.

[16] R. Huiskes and H. Weinans. The Relationship Between Stress Shielding and Bone Resorption Around Total Hip Stems and the Effects of Flexible Materials. *Biomechanics Section, Institute for Orthopaedics*, 274:124–134, 1991.

[17] Liza J. Raggatt and Nicola C. Partridge. Cellular and molecular mechanisms of bone remodeling. *Journal of Biological Chemistry*, 285(33):25103–25108, 2010.

[18] Bone Remodeling Structure And Function Of The Musculoskeletal System Minimalist.

[19] T John Martin. Bone remodelling : its local regulation and the emergence of bone fragility. *Best Practice & Research Clinical Endocrinology & Metabolism*, 22(5):701–722, 2008.

[20] H. M. Frost. Wolff's Law and bone's structural adaptations to mechanical usage: an overview for clinicians. *Angle Orthodontist*, 64(3):175–188, 1994.

[21] William F. Zimmerman, Mark A. Miller, Richard J. Cleary, Timothy H. Izant, and Kenneth A. Mann. Damage in total knee replacements from mechanical overload. *Journal of Biomechanics*, 49(10):2068–2075, 2016.

[22] H. Wiskott and C. Belser. Lack of integration of smooth titanium surfaces. *Clinical Oral Implant Research*, pages 429–444, 1999.

[23] R. Ruimerman. *Modeling and Remodeling in Bone Tissue*. PhD thesis, Technische Universiteit Eindhoven, 2005.

[24] Alun Wall and Tim Board. The compressive behavior of bone as a two-phase porous structure. In *Classic Papers in Orthopaedics*, volume 59, pages 457–460. oct 2014.

[25] Andrew J. Peacock. *Handbook of polyethylene: structures: properties, and applications*. Marcel Dekker, 2000.

[26] Philip D. Harvey. *Engineering Properties of Steel*. American Society for Metals, 1982.

[27] Donald T Reilly and Albert H Burstein. The Mechanical Properties of Cortical Bone. *The Journal of Bone and Joint Surgery*, 56(5):1001–1022, 1974.

[28] C.˜R. Jacobs, M.˜E. Levenston, G.˜S. Beaupre, J.˜C. Simo, and D.˜R. Carter. Numerical instabilities in bone remodling simulations: The advantage of a node-based finite element approach. *J. Biomech.*, 28(4):449–459, 1995.

[29] Jonathan Black and Garth Hastings. CoCr-based alloys. In *Handbook of Biomaterial Properties*, pages 167–178. Springer US, Boston, MA, 1998.

[30] J. Folgado. *Modelos computacionais para Análise e Projecto de Próteses Ortopédicas*. PhD thesis, Instituto Superior Técnico, 2004.

[31] D. Martin. Femoral head prosthesis, 1952.

[32] GrabCAD.

[33] K L Ong. Biomechanics of the Birmingham hip resurfacing arthroplasty. *Journal of Bone and Joint Surgery - British Volume*, 88-B(8):1110–1115, 2006.

[34] M. A. Pérez, P. A. Vendittoli, M. Lavigne, and N. Nuño. Bone remodeling in the resurfaced femoral head: Effect of cement mantle thickness and interface characteristics. *Medical Engineering and Physics*, 36(2):185–195, 2014.

[35] Stephan Rothstock, Anne Uhlenbrock, Nicholas Bishop, Lindsay Laird, Roman Nassutt, and Michael Morlock. Influence of interface condition and implant design on bone remodelling and failure risk for the resurfaced femoral head. *Journal of Biomechanics*, 44(9):1646–1653, 2011.